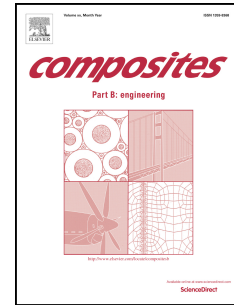


Accepted Manuscript

Multiscale modeling of interphase in crosslinked epoxy nanocomposites

Byungjo Kim, Joonmyung Choi, Seunghwa Yang, Suyoung Yu, Maenghyo Cho



PII: S1359-8368(16)30438-3

DOI: [10.1016/j.compositesb.2017.03.059](https://doi.org/10.1016/j.compositesb.2017.03.059)

Reference: JCOMB 4993

To appear in: *Composites Part B*

Received Date: 21 April 2016

Revised Date: 15 March 2017

Accepted Date: 17 March 2017

Please cite this article as: Kim B, Choi J, Yang S, Yu S, Cho M, Multiscale modeling of interphase in crosslinked epoxy nanocomposites, *Composites Part B* (2017), doi: 10.1016/j.compositesb.2017.03.059.

This is a PDF file of an unedited manuscript that has been accepted for publication. As a service to our customers we are providing this early version of the manuscript. The manuscript will undergo copyediting, typesetting, and review of the resulting proof before it is published in its final form. Please note that during the production process errors may be discovered which could affect the content, and all legal disclaimers that apply to the journal pertain.

Multiscale modeling of interphase in crosslinked epoxy nanocomposites

Byungjo Kim^a, Joonmyung Choi^a, Seunghwa Yang^b, Suyoung Yu^c
and Maenghyo Cho^{a,*}

^a*School of Mechanical and Aerospace Engineering, Seoul National University, 1 Gwanak-ro,
Gwanak-gu, Seoul 08826, Republic of Korea*

^b*School of Energy Systems Engineering, Chung-Ang University, 84 Heukseok-ro, Dongjak-gu,
Seoul 06974, Republic of Korea*

^c*Samsung Electronics, 1-1 Samsunjeonja-ro, Hwaseong, Gyeonggi 18448, Republic of Korea*

Abstract

A multiscale modeling approach is proposed to characterize the interfacial behavior and the interphase properties of epoxy nanocomposites. The interfacial characteristics between the filler and matrix are investigated using molecular dynamics (MD) and molecular mechanics (MM) simulations. With increasing crosslink conversions, the interfacial adhesion between the filler and matrix is reduced which is attributed to the changes of inherent non-bond interaction characteristics at the interface, resulting in retarded reinforcing effect on the stiffness and thermal stability of epoxy nanocomposites. Moreover, to understand the structural change in the interphase region of nanocomposites with crosslinking, the radial density profile, the local crosslinks distribution, and the free volume at the filler surface are further examined. The results of structural features consistently demonstrate that the structural conformation of the interphase is substantially influenced by the reduction of interfacial communication with increasing crosslink conversion. In order to take into account the variations of interfacial compliance and the thermomechanical property of the interphase region, the effective interphase concept is implemented. Further, the micromechanics-based multi-inclusion model provides a reasonable prediction for the thermomechanical property of composites using the effective interphase concept.

Keywords: Multiscale modeling, Crosslink conversion, Interphase, Nanocomposites, Molecular dynamics simulation

1. Introduction

Polymer crosslinking has extended engineering applications of polymer materials providing enhanced performances compared to the linear polymers. Epoxy resins, defined as thermoset polymers, exhibit high specific stiffness, high strength, thermal stability, and chemical resistance property due to the crosslinked polymer networks by strong covalent bonds [1]. In addition to excellent property, the ease of processing of epoxy offers various applications for matrix materials with the incorporation of reinforcing fillers [2-4]. The fundamental characteristics of epoxy resins are substantially modified according to the degree of crosslinking [5]. It is well known that the spatial constraints imposed by the network junctions restrict the polymer chain dynamics and the conformation freedom which is associated with the glass transition temperature (T_g) changes with crosslinking. Experimental and theoretical works reported that T_g increases with crosslinking conversions, since the crosslinked topology induces strong connectivity between polymer segments [1, 6]. When reinforcing filler materials are introduced to the crosslinked polymers, the dynamics of polymer networks become more complicated, in particular at the surface of fillers due to the addition of the interactions of polymer chains with the embedded particulates [6-8].

The region of the polymer matrix near the filler surface is typically termed the interphase, where polymer-filler interactions modify the dynamics and physical properties of polymer segments. With decreasing filler dimensions to a nanometer scale, the polymer dynamics change as the interfacial interactions become prominent since nanoparticles have an extremely high surface area to volume ratio [3]. Moreover, while a relatively small interphase

region exists in conventional micron-filled composites, it has been demonstrated that with the presence of well-dispersed nanofillers in the polymer matrix, the interphase zones can percolate into the entire nanocomposites system, thus dominating the bulk polymer properties [6, 9-11]. The effects of nanoscale confinement on the surrounding polymer matrix for polymer nanocomposites systems have been studied through experiments, which have been found to be manifested by the change in T_g of the polymer matrix in comparison to the neat polymer. In the literature, increased or suppressed T_g of polymers with nanofillers can be found depending on the nature of the interfacial interactions [6, 12-16], indicating that the polymer mobility is substantially influenced by the interfacial communication between the filler and matrix. It has been reported that the unfavorable interactions at the interface result in decreased T_g [14-16] and interphase-like behavior attributed to relatively strong interfacial interactions may improve T_g [6, 12, 13]. However, conclusive agreement has not yet been reached regarding the detailed mechanism behind these variations of T_g regarding the effect of interfacial interactions for epoxy matrix with nanofillers.

In order to predict and control the properties of polymer nanocomposites quantitatively, the interfacial region needs to be characterized in terms of the various design parameters considered in the nanocomposites systems. Based on the general agreement that the formation of the interphase zones is attributed to the retarded polymer dynamics by the interfacial interactions between the fillers and polymer matrix [9, 17], the interphase creation and the interfacial characteristics of nanocomposites with crosslinked polymer need profound consideration, since the polymer dynamics near the surface are simultaneously influenced by the interfacial interactions and the crosslinked network topology [6-8]. While the perturbations of local structural and dynamical properties of thermoplastic polymer matrix surrounding embedded nanofillers have been intensively investigated by experimental and

computational methods [18, 19], understanding of the interphase zones of nanocomposites with crosslinked polymer is still limited.

The nature of experiments makes it challenging to independently distinguish one effect from many parameters that affect the properties of nanocomposites, such as the interfacial characteristics and the interphase properties in epoxy nanocomposites. Regarding this aspect, molecular dynamics (MD) simulations have been used to provide valuable insights for understanding polymer physics especially in the interfacial zone of nanocomposites systems with thermoset matrix [13, 20-23]. Li *et al.* [24] performed MD simulations to investigate the interfacial region of crosslinked epoxy with multilayer graphene, focusing on the different orientations of graphene layers. Hadden *et al.* [7] presented the MD simulation work regarding the influence of crosslink density on the molecular structure of the interface for the graphite fiber/epoxy matrix. They demonstrated that the effective surface thickness from the graphene sheet is insensitive to the variation of crosslinking. Recently, quantitative assessment on the interfacial interactions of epoxy nanocomposites with the effect of crosslink conversion was carried out by the present authors [25], indicating that the interfacial adhesions at the surface of nanofillers decrease with increasing crosslink conversions. Beyond the atomistic level observation in MD simulations, the coarse graining (CG) MD simulations have provided the interfacial nature between epoxy and a generic surface in a mesoscale perspective. Langeloth *et al.* [26] performed CG MD simulations to examine the characteristics of the interphase of crosslinked epoxy and a metallic surface.

Together with the MD simulations, a multiscale framework combined with a continuum regime has offered effective ways to understand nanoscale physics regarding the interphase in composite systems. Odegard *et al.* [27] developed a three-phase continuum model that demonstrates the interphase properties with various surface treatments of nanoparticles. Cho

and his collaborators [28-30] presented a detailed particle size effect on the interphase using multiscale modeling approaches with MD simulations and a micromechanics model. Regarding the interfacial debonding in heterogeneous medium, Safaei *et al.* [31] investigated the damage of the interface induced from the interfacial debonding for graphite nanoplatelet polymer composites using the cohesive zone model while implementing the MD simulation work conducted by Awasthi *et al.* [32]. Zappalorto *et al.* [33] proposed a multiscale model to describe the damage mechanisms in nanoscale which is associated with the nanoparticle debonding with considering the presence of the interphase zone.

In this paper, starting from the MD study presented in the previous work [25], a multiscale model is proposed to illustrate the effect of crosslinking as well as filler sizes on the interfacial region. The present multiscale model takes into account the variations of interfacial characteristics and interphase properties with the degree of curing conversions and nanoparticle sizes, reflecting nanoscale physics observed in atomic scale simulations. The primary purpose of the study, with the incorporation of MD simulations and a micromechanics model, is to develop a systematic computational study on the interphase region and interfacial characteristics of epoxy nanocomposites considering the influence of crosslink conversions and filler sizes.

2. Molecular simulations results

This section briefly introduces the procedure for establishing the molecular models and implementing ensemble simulations. Commercial molecular simulation software, Material Studio 5.5 [34], was employed for the molecular modeling and ensemble simulations used herein. To describe both inter- and intra-atomic interactions, the COMPASS (*ab initio*

Condensed-phase Optimized Molecular Potential for Atomistic Simulation Studies) forcefield [35] was used. The results of MD and MM simulations in our previous work regarding the interfacial characteristics are further discussed considering varying crosslink conversions and nanoparticle sizes.

2.1 Molecular modeling

For establishing crosslinked epoxy structures composed of epoxy resin EPON 862 and curing agent TETA, the representative molecule method was used with varying crosslink conversion degrees of 16.67%, 33.33%, 50.00%, and 62.50%. A detailed procedure for crosslinking was described in our previous work [25]. For epoxy nanocomposite structures, the spherical shape of silica nanoparticles having the radius of 6.60 Å, 8.25 Å, and 10.1 Å were chosen as reinforcing materials without considering any surface treatments or covalent grafting. The Amorphous Cell module[®] was used to construct unit cells for neat epoxy and nanocomposites. The target densities of 1.2 g/cm³ were set for both pure epoxy and nanocomposites systems and the filler volume fractions of 5.6% were considered for epoxy/silica nanocomposites. To remove any finite size effects of unit cells, the periodic boundary conditions were imposed in all directions. The detailed compositions of unit cells for pure epoxy and nanocomposites are presented in **Table 1**. The unit cells were then minimized using the conjugate gradient method. To achieve equilibrated unit cells, 200 ps of *NVT* (isothermal) ensemble at 300 K and 2000 ps of *NPT* ensemble (isothermal and isobaric) at 300 K and 1 atm were applied consecutively. The configuration of the molecular model for pure epoxy and epoxy/silica nanocomposites is illustrated in **Fig. 1**.

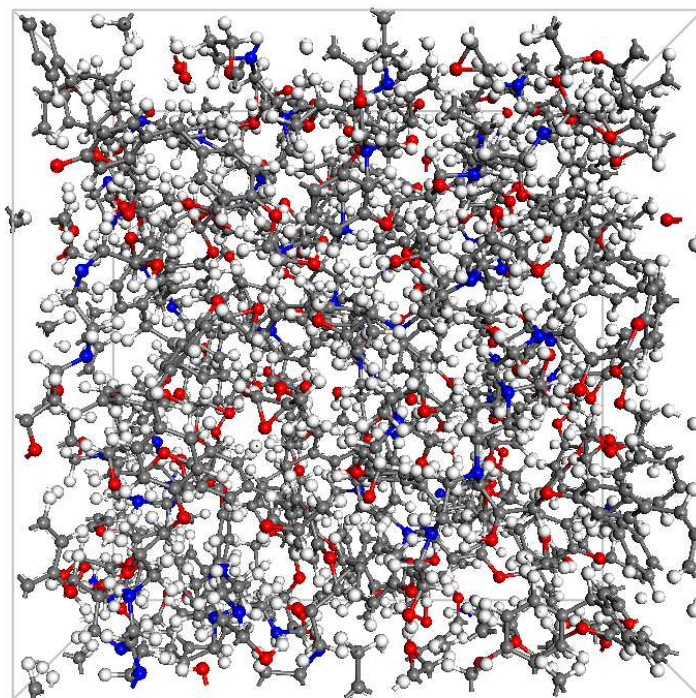
Table 1

Compositions of neat epoxy and epoxy/silica nanocomposite unit cells.

Radius of particle [Å]	Crosslink conversion* [%]	No. EPON 862	No. of TETA	No. of crosslinks /No. of possible crosslinks	Cell length [Å]	Particle volume fraction
6.60	16.66	36	12	12/72	27.84	0.056
	33.33	36	12	24/72	27.84	0.056
	50.00	36	12	36/72	27.84	0.056
	62.50	36	12	45/72	27.84	0.056
8.25	16.66	72	24	24/144	34.79	0.056
	33.33	72	24	48/144	34.79	0.056
	50.00	72	24	72/144	34.79	0.056
	62.50	72	24	90/144	34.79	0.056
10.10	16.66	132	44	44/264	42.55	0.056
	33.33	132	44	88/264	42.55	0.056
	50.00	132	44	132/264	42.55	0.056
	62.50	132	44	165/264	42.55	0.056
Neat epoxy	16.66	48	16	16/96	27.84	-
	33.33	48	16	32/96	27.84	-
	50.00	48	16	48/96	27.84	-
	62.50	48	16	60/96	27.84	-

Crosslink conversion* is defined as the ratio of crosslinking reactions over total possible reactions.

(a)



(b)

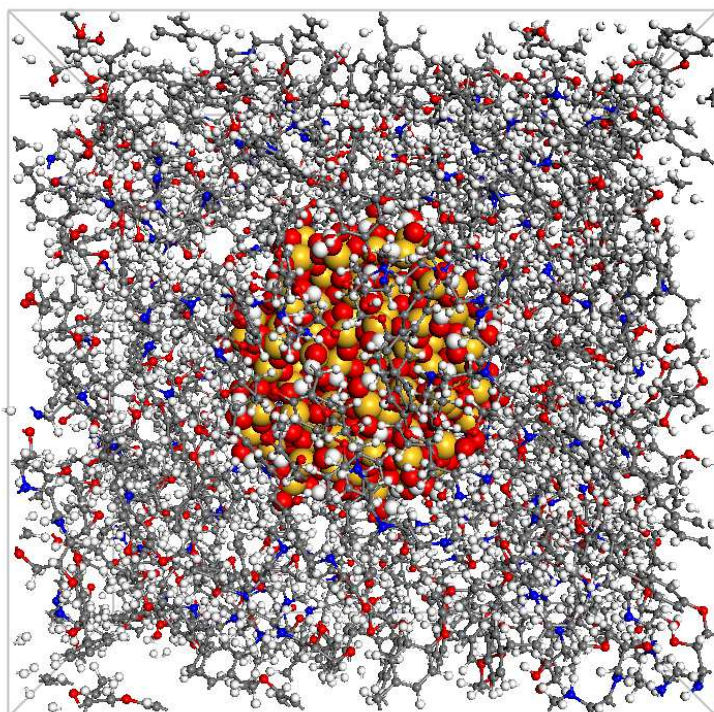


Figure 1. Configuration of molecular unit cell structure for (a) pure epoxy and (b) epoxy/silica nanocomposites.

2.2 Thermomechanical property

To examine the variation of enhancement effects on the thermomechanical property in nanocomposites, the elastic modulus and the coefficient of thermal expansion (CTE) of equilibrated unit cells were predicted using production runs with proper ensemble simulations. The elastic moduli of epoxy and nanocomposites were obtained using the Parrinello-Rahman strain fluctuation method with the incorporation of the $N\sigma T$ (constant stress) ensemble that allows both normal deformations and distortions of unit cells [36, 37]. Following the fluctuation scheme, both neat epoxy and nanocomposites unit cells were further equilibrated at 300 K and 1 atm of the diagonal components of internal stress tensor for 500 ps. To collect the fluctuations of both normal and shear strain components, the same $N\sigma T$ ensemble was applied for 100 ps and all thermodynamic quantities were stored at each 10 fs. From the information collected in the final production run, the elastic stiffness tensor C_{ijkl} of the unit cell is given as,

$$C_{ijkl} = \frac{kT}{\langle V \rangle} \langle \delta \varepsilon_{ij} \delta \varepsilon_{kl} \rangle^{-1} \quad (1)$$

where ε_{ij} , V , and T are the strain tensor, volume, and temperature of the unit cell and k is the Boltzmann constant. From eight different final production runs, the elastic moduli of each unit cell were averaged to compensate for the inherent computational fluctuations in the MD simulations. To confirm the temperature dependency on the mechanical properties, the elastic moduli for both neat epoxy and nanocomposites (of $r_p = 6.6 \text{ \AA}$ and 10.1 \AA) systems were further calculated for a range of temperature for the glassy region with following the same manner as described previously.

In order to quantify the variation of thermal stability with crosslink conversions and filler sizes, the CTEs of epoxy and nanocomposites were calculated at a temperature range of

glassy state. The equilibrated unit cells were heated to 350 K using the *NPT* ensemble. During a stepwise cooling-down procedure with the cooling rate of 20 K/1000 ps of the *NPT* ensemble, the averaged volume-temperature of each unit cell was monitored at every 20 K. The coefficient of linear thermal expansion (CLTE), α , was calculated using a linear regression of the temperature-volume relation:

$$\alpha \cong \frac{\beta}{3} = \frac{1}{3V_0} \left(\frac{\partial V}{\partial T} \right)_p \quad (2)$$

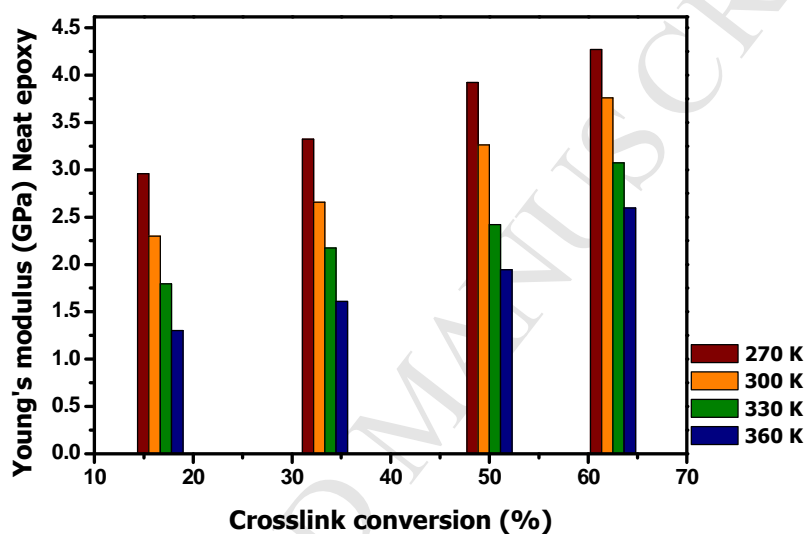
where β is the coefficient of volumetric thermal expansion (CVTE) and V_0 is the reference volume of the unit cell at 300 K.

The elastic properties of neat epoxy and nanocomposites for a range of temperature from 270 K to 360 K are compared in **Fig.2**. As can be expected, with increasing temperature the Young's modulus tends to decrease for both neat epoxy and nanocomposites systems. As far as the overall trend with the degree of crosslinking is concerned, the temperature-dependent elastic properties show a similar tendency with crosslinking at the temperature range within the glassy region. In the present work, the elastic properties for neat epoxy and nanocomposites at atmospheric temperature (300 K) are thoroughly discussed.

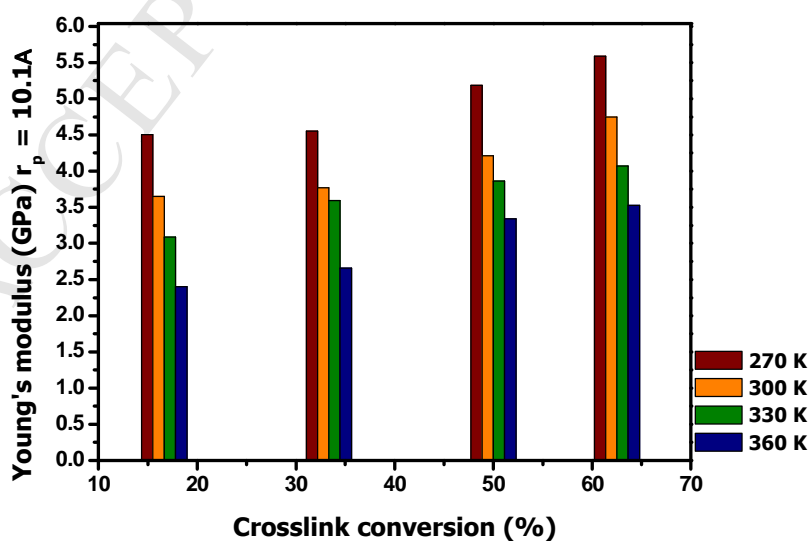
The results of elastic moduli at 300 K and CTEs from the MD simulations are listed in **Table 2-4** with the values predicted from the Mori-Tanaka model. Compared to the Mori-Tanaka solutions, the Young's modulus and shear modulus of the nanocomposites exhibit seemingly higher values while showing lower values for CTEs, indicating that the two-phase Mori-Tanaka micromechanics model, without considering the interphase, cannot predict the properties of nanocomposites reasonably. However, the Mori-Tanaka solutions compared to the MD results provide important physical insights regarding the interphase effects, since the deviations between the MD results and the Mori-Tanaka solutions are directly attributed to

the properties of the interphase region. As can be seen in **Tables 2-4**, the deviations decrease as the conversion degrees and the filler sizes increase, inherently demonstrating that the interphase characteristics for reinforcing effects are likely to be disturbed with increasing crosslinking and filler sizes.

(a)



(b)



(c)

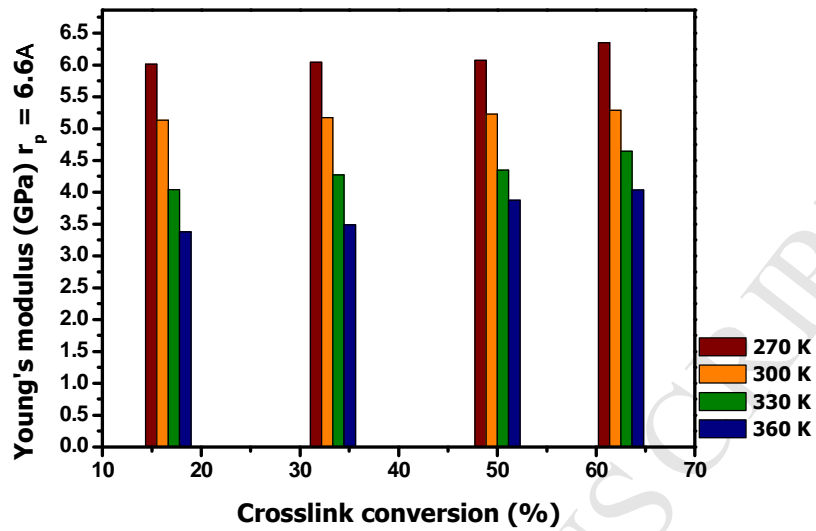


Figure 2. Young's modulus of neat epoxy and nanocomposites with the degree of crosslinking for a range of temperature (from 270 K to 360 K within the glassy region of epoxy); (a) neat epoxy, (b) $r_p=10.1 \text{ \AA}$, and (c) $r_p=6.6 \text{ \AA}$.

Table 2

Young's modulus of neat epoxy and nanocomposites with the Mori-Tanaka model.

Particle radius [\AA]	Crosslink conversion [%]			
	16.66	33.33	50.00	62.50
6.60	5.13 ± 0.30	5.17 ± 0.41	5.23 ± 0.52	5.29 ± 0.36
8.25	3.94 ± 0.26	4.23 ± 0.42	4.47 ± 0.47	4.90 ± 0.38
10.10	3.65 ± 0.29	3.77 ± 0.30	4.21 ± 0.33	4.75 ± 0.31
M-T	2.58	2.97	3.64	4.19
Neat epoxy	2.30 ± 0.16	2.66 ± 0.29	3.26 ± 0.46	3.76 ± 0.36

Table 3

Shear modulus of neat epoxy and nanocomposites with the Mori-Tanaka model.

Particle radius [Å]	Crosslink conversion [%]			
	16.66	33.33	50.00	62.50
6.60	1.93 ± 0.13	1.94 ± 0.16	1.95 ± 0.21	1.97 ± 0.15
8.25	1.45 ± 0.11	1.57 ± 0.16	1.64 ± 0.19	1.82 ± 0.15
10.10	1.33 ± 0.12	1.37 ± 0.12	1.54 ± 0.13	1.74 ± 0.11
M-T	0.92	1.11	1.13	1.53
Neat epoxy	0.82 ± 0.12	0.96 ± 0.12	1.18 ± 0.17	1.37 ± 0.14

Table 4

Thermal expansion coefficient (CTE) of neat epoxy and nanocomposites with the Mori-Tanaka model.

Particle radius [Å]	Crosslink conversion [%]			
	16.66	33.33	50.00	62.50
6.60	112.98	104.79	85.02	73.00
8.25	127.99	118.90	104.89	78.83
10.10	134.06	121.38	110.11	81.14
M-T	144.77	126.96	112.29	84.29
Neat epoxy	155.50	136.47	120.77	90.72

2.3 Change in interfacial characteristics

The MD simulation results in the previous section offer important predictions in terms of the interphase effect with crosslinking and filler sizes. That is, the interphase effect tends to decrease with increasing crosslinking densities and embedded particle sizes. To clarify the variations of interfacial reinforcing effect with the design parameters considered in this work, the interfacial characteristics were rigorously examined using MD and MM simulations. In this section, the MD and MM simulation results regarding the interfacial characteristics reported in the previous work have been revisited and extended.

In the present molecular models without considering any surface modifications, non-bond

interactions between the silica particle and epoxy matrix govern the communication of interfacial dynamics, which play a key role in determining the interphase characteristics. To evaluate the changes of intrinsic adhesion strength at the interface with varying crosslink conversions and filler sizes, the non-bond interfacial interaction energy/unit volume was calculated from the equilibrated unit cells, defined as:

$$\rho_{interaction} = \frac{E_{composite} - (E_{particle} + E_{matrix})}{V_{particle}} \quad (3).$$

where $E_{composite}$, $E_{particle}$, and E_{matrix} denote the potential energy of the nanocomposite, particle, and matrix, respectively, each of which was obtained from the single point energy of the final configuration of nanocomposites after the equilibration process, and $V_{particle}$ is the volume of particle for each nanocomposite

The interfacial interaction energy density (see **Fig. 2**), where the negative values of non-bonding energy represent the interfacial attraction of the polymer matrix with the silica particle, provides an important physical interpretation regarding the variation of interfacial attraction with the particle size and crosslinking conversion. As the embedded filler size decreases, the particle tends to entail high non-bonding interaction energy density, which corresponds to the increasing number of non-bonding pairs per unit volume of particle. Interestingly, the interfacial adhesive interactions between the particle and matrix are weakened by the presence of more crosslinks. The highly crosslinked epoxy matrix is relatively less attractive to the silica surface than the matrix with lower conversion degrees. This behavior is most likely due to the disturbed interfacial communications at the particle surface with increasing crosslinking conversion.

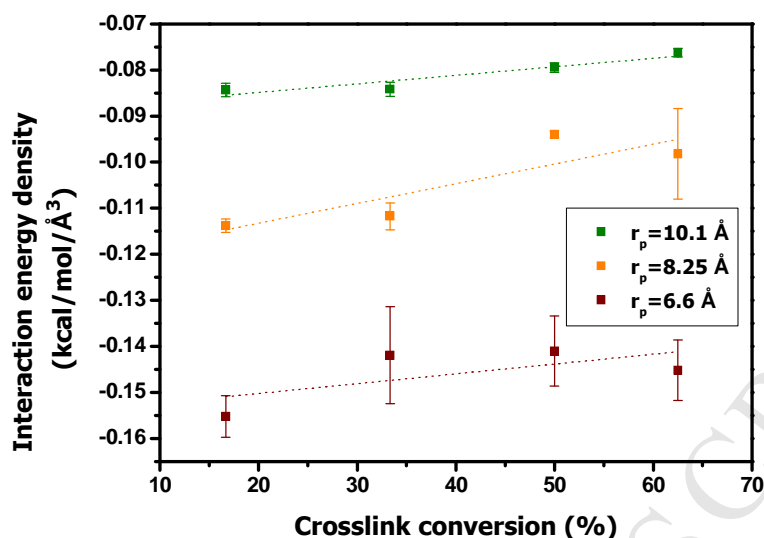


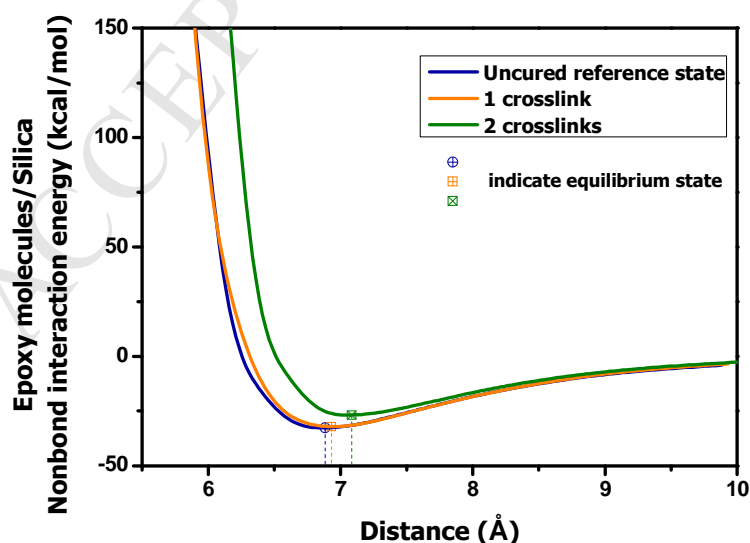
Figure 3. Interfacial interaction energy density of crosslinked epoxy/silica nanocomposites with different crosslink conversions; Reproduced with permission from Elsevier [25].

Previous work [25] using MM simulations revealed that the degradation trend of interfacial adhesion to the silica surface with crosslinking is attributed to the alternation of atomic connectivity after crosslinking reactions. From a simple molecular structure consisting of a planar silica layer, one molecular of EPON 862, and two molecules of TETA, the changes of non-bond characteristics between epoxy have been observed. As can be seen in **Fig. 3 (a)**, non-bond characteristics between epoxy molecules and silica are altered with curing degrees compared to the uncured reference state; the magnitude of the attractive non-bond interactions of epoxy to the silica surface decreases, and the equilibrium distance between the epoxy molecules and the silica gradually increases with producing more crosslinks. This interfacial degradation with crosslinking is supported by the variation of non-bond characteristics of participating atoms during the curing reaction as given in **Fig. 3 (b)**. In the uncured reference state, the N-C-O atoms (the specific part of resin and hardener involving the crosslinking reaction with atomic connectivity changes) have intrinsically repulsive

interfacial characteristics (positive sign) to the silica surface. With the formation of crosslinks, new covalent bonds between C and N atoms are formed, accompanied with the valence changes of the N-C-O atoms, increases in the magnitude of repulsion between the N-C-O and silica, and further increases in the equilibrium distance.

This MD and MM simulation result offers an important insight into the nature of interfacial communications at the surface especially with crosslinking which is governed by the non-bond interactions between the epoxy and silica. As the number of crosslinks increases, the repulsive interactions of participating atoms (N-C-O) with silica gradually increase, inducing the degradation of interfacial interactions in highly crosslinked epoxy nanocomposites. Since the interphase properties are strongly influenced by the non-bond interactions at the interface in this study, the variations of interfacial interactions during the crosslinking reaction demand a thorough consideration to understand the interphase characteristics of crosslinked epoxy nanocomposites.

(a)



(b)

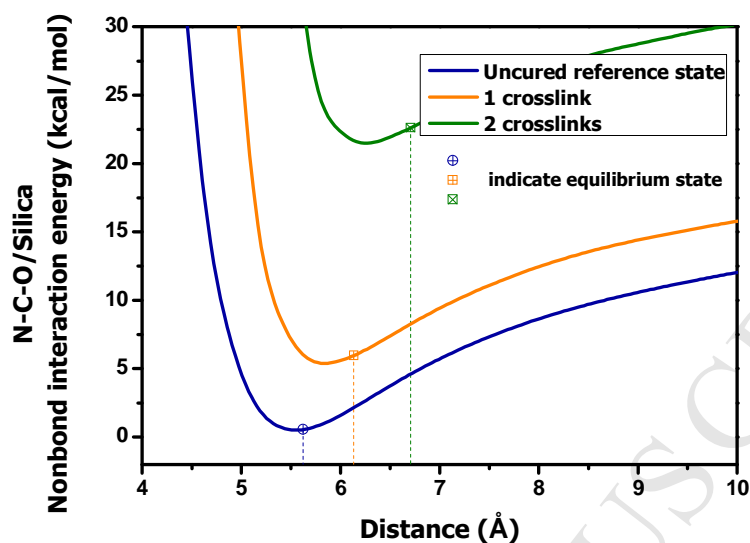


Figure 4. Variation of non-bond characteristics (a) between epoxy molecules and silica, and (b) between N-C-O atoms and silica with crosslinking reaction; Reproduced with permission from Elsevier [25].

2.4 Change in structural characteristics of interphase

To provide more detailed discussion of the interphase region with the degree of crosslinking, the radial density profile, the local crosslinks distribution, and the free volume at the filler surface were further investigated. In **Fig.5**, the radial mass density profile from the center of nanoparticle $r_p=10.1$ Å are compared with crosslinking. The peak densities are observed in the vicinity of the filler and the density profiles begin to converge toward the bulk matrix region around 7 Å from the particle surface. Similar to the work by Hadden et al. [7], distinct differences in the thickness of interphase with varying crosslink conversion are not observed. Based on the observation in the radial density profile for nanocomposites ($r_p=6.6$ Å, 8.25 Å, and 10.1 Å), we defined the thickness of interphase region as 6.9 Å which is a reasonable value as compared to the literatures [7, 12, 30, 38, 39].

From the magnified view in the peak region (**Fig. 5**), important features can be observed

with increasing crosslink conversion of epoxy. As the degree of crosslinking increases, the peak magnitudes of density profile tend to decrease. Moreover, the distances where the peak amplitudes appear are slightly increased from the filler surface with the formation of more crosslinks. This result demonstrates that the interfacial effect between the filler and matrix is disturbed with the formation of more crosslinks since the polymer networks tend to experience more spatial constraints by crosslinking. A similar trend was reported by Hadden et al. [7] and the reduction of interfacial interaction with the crosslink density (Figs. 3 and 4) can also support this result.

Fig. 6 shows the local crosslinks distribution along the radial direction for the nanocomposites of $r_p=10.1 \text{ \AA}$. The local crosslinks distribution profiles were determined using the number of carbon atoms associated with crosslinking reactions per the volume with the radial direction. The result demonstrates that lower crosslink conversion zones can be observed in the interphase region nearby the filler surface. As we observed in **Fig. 4**, the MM calculation result revealed that with the formation of more crosslinks the repulsive interfacial interactions between the silica surface and the participating atoms in crosslink reactions increase. Thus, the local crosslinks distributions are likely to be lowered at the interfacial region around the filler surface as compared to bulk epoxy matrix.

The free volume is one of important features which represent the structural characteristics of amorphous polymer networks. Herein, the free volume was calculated based on the Connolly surfaces algorithm [40, 41] with the Connolly probe sphere radius of 1 \AA and the van der Waals radius of 9.5 \AA . The overall free volume was obtained from the outside space of the occupied volumes of polymer networks, and the interfacial free volume was determined by the summation of the free volume segments at the filler surface. Free volume evolution with the crosslink conversion for the nanocomposites of $r_p=10.1 \text{ \AA}$ is given in **Fig.**

7. As shown in **Fig. 7**, with the increasing conversion ratio the free volume at the surface tends to increase as well as the overall free volume of nanocomposites. It is natural that the overall free volumes of nanocomposites increase with crosslinking, since the polymer networks are more secured by the presence of more crosslinks so that more voids can be formed between the polymer chains [42]. An interesting feature to be noted is that the interfacial free volumes increase with the crosslink conversion. The interfacial free volume represents the voids at the interfacial region, thus an increase in the interfacial free volumes with increasing crosslink conversion are directly attributed to the reduction of interfacial adhesion between the filler and matrix (in agreement with the result shown in **Fig. 3**). Moreover, the fraction of the interfacial free volume to the overall free volume increases from 0.91% to 2.55%. An increase in the fraction of the interfacial free volume indicates that in a qualitative sense the disturbed interfacial interaction with crosslinking induces a significant change in the interfacial structure of nanocomposites as compared to the inherent overall free volume evolution of epoxy matrix with the formation of more crosslinks.

The structural features discussed herein can be regarded as important evidence of how the interphase regions of nanocomposites are influenced by crosslinking in terms of the structural point of view. Those observations are also consistent with the previous MD and MM results (see **Fig. 3** and **Fig. 4**) which indicate the reduction of interfacial interaction with increasing crosslink conversion.

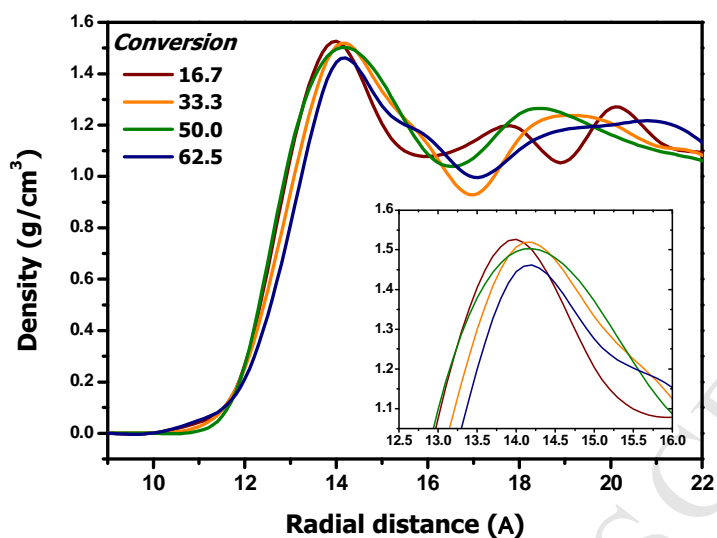


Figure 5. Radial mass density profile along the radial direction from the center of nanoparticle ($r_p=10.1 \text{ \AA}$).

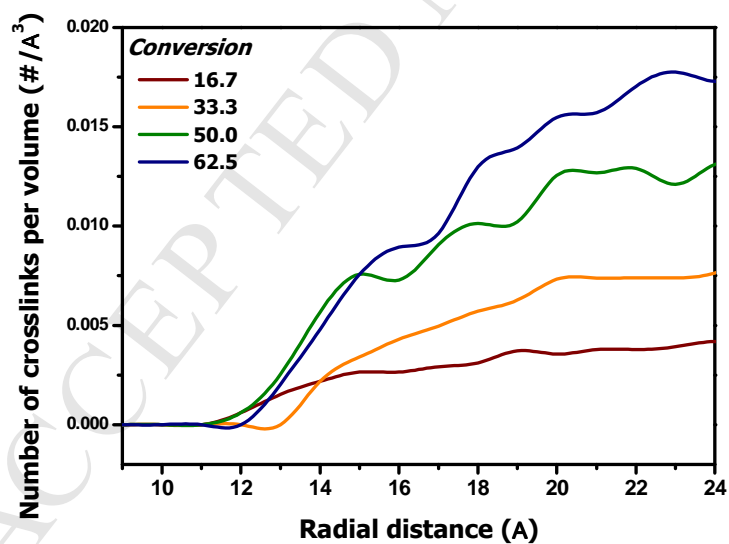


Figure 6. Local crosslinks distribution as a function of crosslink conversion along the radial direction from the center of nanoparticle ($r_p=10.1 \text{ \AA}$).

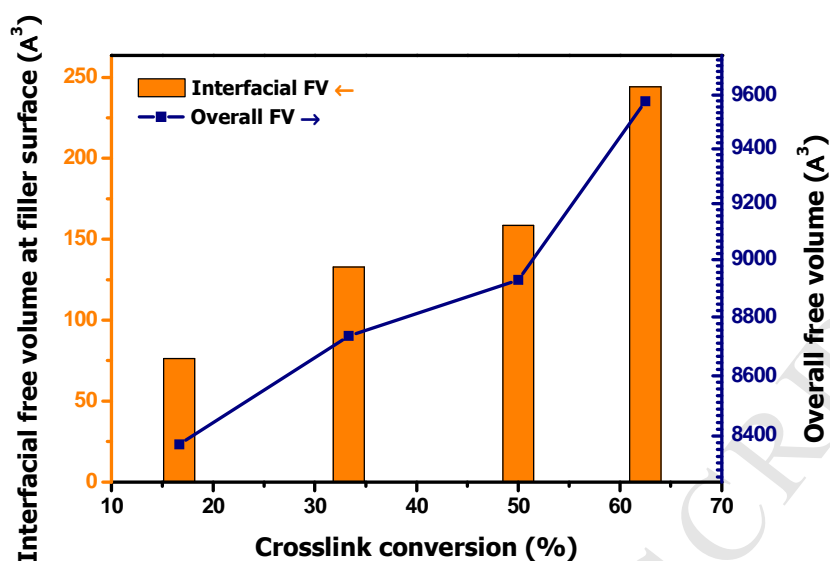


Figure 7. Interfacial free volume in the vicinity of filler surface and overall free volume of nanocomposites ($r_p=10.1 \text{ \AA}$).

3. Multiscale modeling

3.1 Brief review of multiscale modeling in nanocomposites

Multiscale modeling strategy combined with continuum models has been widely used to understand the structure-property relationship of nanocomposites. Based on the observations that the interphase region shows distinguishably different properties than those of the bulk polymer matrix [6, 7, 17], the interphase zone has been modeled in continuum models as an independent layer between the embedded filler and matrix with the incorporation of a fictitious infinite medium [27, 28, 30, 33, 43-48]. With a profound consideration on the interphase region in conventional micromechanics models (the Mori-Tanaka model, the Halpin-Tsai equation, etc.), a wide range of nanoscale phenomena associated with a distinct nature of interface and interphase in nanocomposites can be taken into account in the continuum scale.

Regarding the nanoparticle size dependent characteristics, termed the particle size effect,

the multi-inclusion models have successfully characterized the properties of various polymer nanocomposites. Yang and Cho [28, 30] derived the interphase properties of nanocomposites in terms of mechanical aspects using multi-inclusion models to characterize the nanoscale size effect with the consideration of the dilute and nondilute concentration effects. Thermal properties including thermal expansion and thermal conductivity of polymer nanocomposites have also been tailored with the micromechanics models combined with MD simulations [38]. Quaresimin and his collaborators [33, 46-48] have significantly contributed to describe the fracture toughness mechanism (nanoparticle debonding, plastic yielding of nanovoids, and plastic shear band of polymer) in polymer nanocomposites using a multiscale modeling strategy with a thorough consideration on the interphase region. For the stress transfer characteristics, a three-phase micromechanical model and finite element analysis strategy was proposed to predict the interfacial stress transfer from the matrix to the fiber in fiber-reinforced composites [49] and carbon nanotube reinforced composites [50, 51]. Recently, the thermo-viscoelastic properties of fiber reinforced polymers are predicted by Rao et al. [52] using a micromechanics regime with the incorporation of graded interphases and imperfect interfaces.

Multiscale modeling strategies with the incorporation of the interphase region have provided valuable insights on nanoscale physics in nanocomposites, however, the interfacial characteristics of epoxy nanocomposites depending on the degree of crosslinking have not yet been considered in the continuum scale. In this section, the multi-inclusion model is addressed to characterize the interfacial region of crosslinked epoxy nanocomposites considering the nanoscale physics of the interphase zone. In this method, the properties of nanocomposites obtained from MD simulations are equated to the micromechanics solution that can predict not only the overall properties of composites but also those of their individual

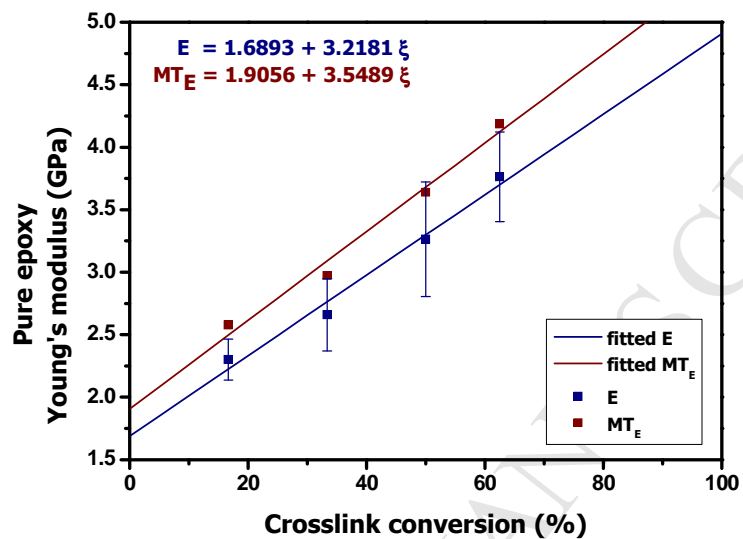
phases.

3.2 Characterization of the property of nanocomposites with conversion degree and filler size

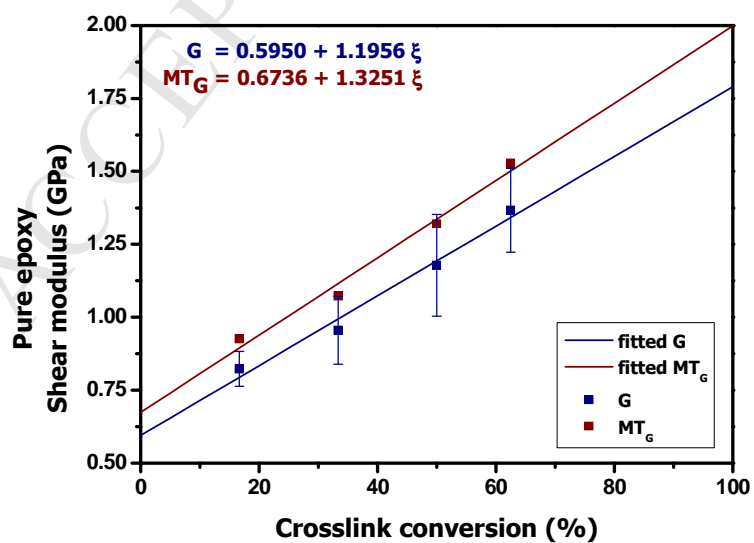
The properties of epoxy/silica nanocomposites as well as their interfacial characteristics have been investigated in terms of crosslink conversions and filler sizes using MD and MM simulations, while demonstrating a clear dependency with respect to the degree of crosslinking and particle size. To characterize those characteristics in the continuum scale, the relationship of the properties of crosslinked neat epoxy systems with crosslinking was first examined. Regarding the thermomechanical properties of epoxy with crosslink conversions, the linear trends of increasing elastic moduli and decreasing CTEs with the curing ratio have been addressed in a previous work [25] using MD simulations in accordance with the literature from experiment [53] and computational works [22, 54-57]. The properties of crosslinked neat epoxy systems $y|_{pure}$ were assumed to be a linear function of crosslink ratio ξ to characterize the crosslinking-dependent properties of bulk epoxy systems. Similarly, followed by the linear relations of the thermomechanical properties of epoxy with crosslink conversions, the Mori-Tanaka solution $y|_{M-T}$ considering the silica particle inclusions were also regarded as a linear function of crosslinking conversion. Thus, Young's modulus, shear modulus, and the CTE of crosslinked epoxy and as well as their Mori-Tanaka solutions were characterized corresponding to a specific conversion ratio as described in **Eq. (4)**. **Fig. 8** represents the variation of the thermomechanical properties of neat epoxy and their Mori-Tanaka solutions with crosslinking degree described by a linear polynomial fit.

$$\begin{aligned} y|_{pure} &= f(\xi) \\ y|_{M-T} &= g(\xi) \end{aligned} \quad (4)$$

(a)



(b)



(c)

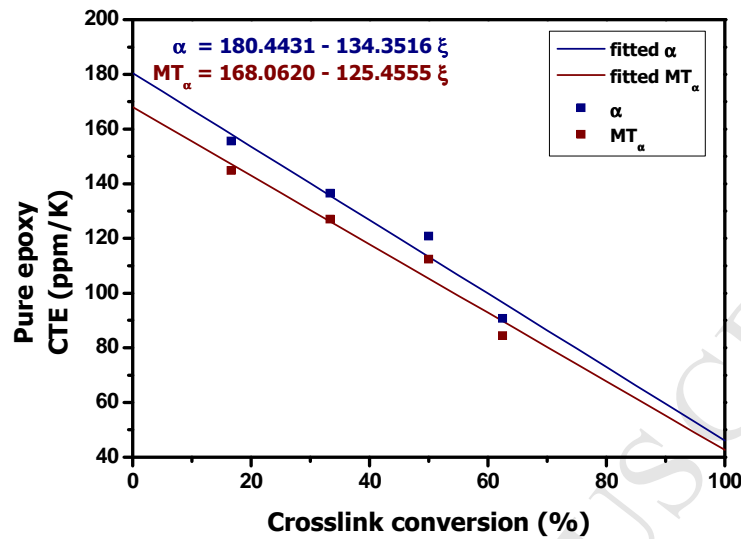


Figure 8. Characterization of thermomechanical properties of crosslinked neat epoxy and their Mori-Tanaka solution (considering the silica particle inclusion with 0.056 of filler volume fraction) with the degree of crosslinking; (a) Young's modulus, (b) shear modulus, and (c) CTE.

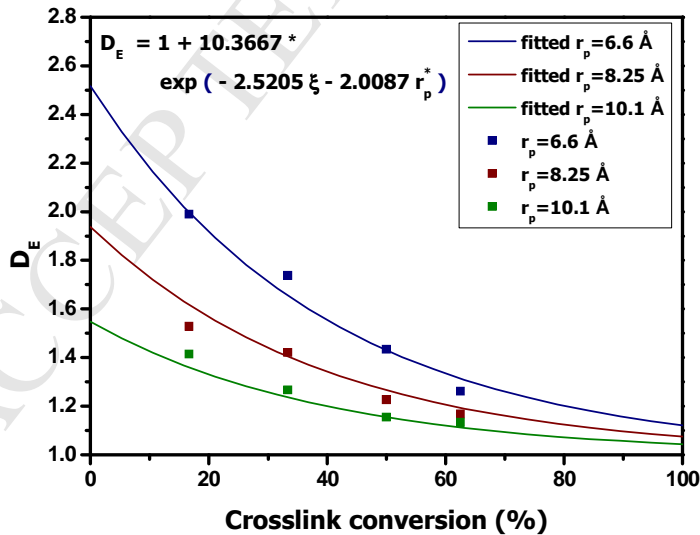
To reflect the variations of properties of epoxy/silica nanocomposites depending on crosslinking and filler size, the degradation factor D is introduced which is defined as the ratio of the properties of nanocomposites $y|_{comp}$ to the Mori-Tanaka solution $y|_{M-T}$. The parameter D inherently represents the interphase effect on the enhancing behavior due to the embedded nanoparticles, since the Mori-Tanaka model based on Eshelby's elasticity solution for inhomogeneity within an infinite medium provides a reference solution for elastic modulus and CTE without considering the interphase region. It has been observed in the previous MD and MM simulations that the interphase effect tends to decrease with increasing crosslinking conversions and decreasing particle sizes. On the basis of this emphasis on the interphase effect, the degradation factor D is characterized in terms of two nondimensional variables, the crosslink conversion ξ and the normalized particle radius r_p^* . The particle

radius for each nanocomposite r_p is normalized by the thickness of interphase t_i , as $r_p^* = r_p / t_i$. For convenience, the t_i for each nanocomposite is assumed to be a constant value of 6.9 Å. To reflect the asymptotical convergence of D for Young's modulus D_E , shear modulus D_G , and CTE D_α with ξ and r_p^* , the degradation factors are fitted using an exponential function as follows,

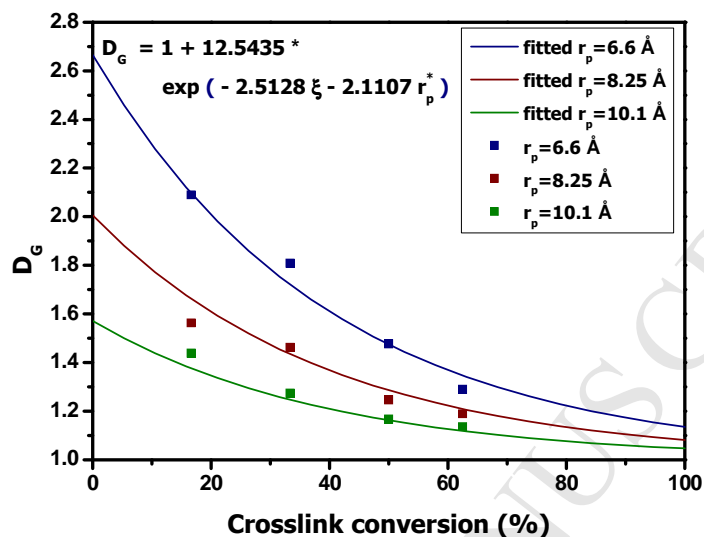
$$D = D(\xi, r_p^*) = 1 + A \exp[-\alpha\xi - \beta r_p^*] \quad (5)$$

where the coefficients A , α , and β for each property are determined with the least-square fitting method. The degradation factor of elastic modulus and CTE for epoxy/silica nanocomposites considered in this study is illustrated in **Fig. 9** with a curve fit as described in **Eq. (5)**.

(a)



(b)



(c)

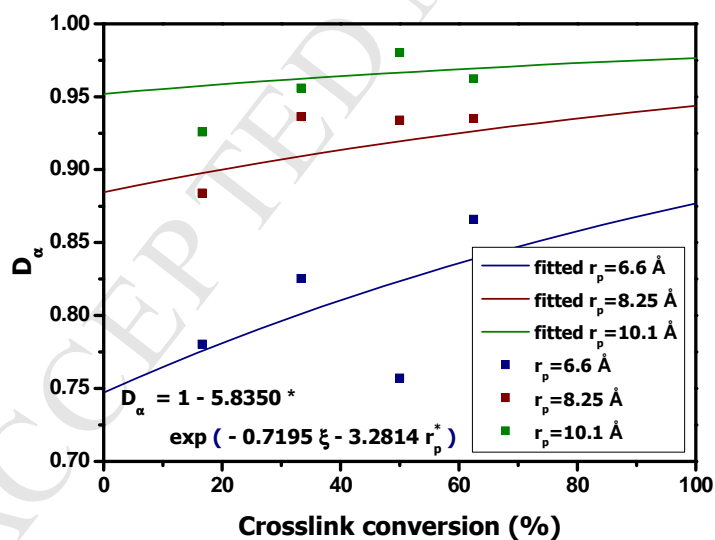


Figure 9. Characterization of degradation factor D for (a) Young's modulus D_E , (b) shear modulus D_G , and (c) CTE D_α with a curve fit by the equation $D(\xi, r_p^*) = 1 + A \exp[-\alpha\xi - \beta r_p^*]$.

As shown in **Fig. 9**, D_E and D_G decrease with increasing crosslink conversion and filler size, which proportionally represent the reinforcing effect with the formation of the interphase on the elastic modulus in epoxy/silica nanocomposites. Meanwhile, D_α gradually increases as crosslinking further proceeds and filler sizes increase, indicating that D_α is inversely proportional to the interphase effect on thermal expansion. By employing **Eq. (5)**, the degradation factors (D_E , D_G , and D_α) demonstrate the contribution of the interphase region to the elastic modulus and CTE of the crosslinked epoxy/silica nanocomposites, corresponding to a specific conversion degree as well as a normalized filler size. Then, the properties of composites $y|_{comp}$ can be given as,

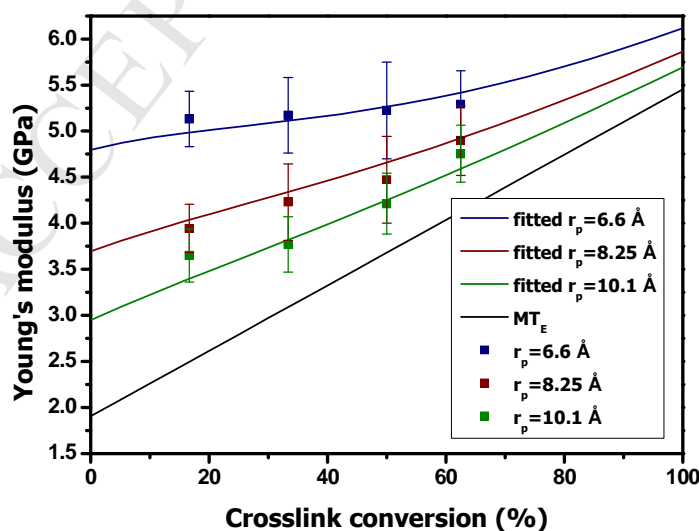
$$y|_{comp} = D(\xi, r_p^*) y|_{M-T} = D(\xi, r_p^*) g(\xi) \quad (6)$$

By adopting the degradation factor and the Mori-Tanaka solution, the thermomechanical properties of the epoxy/silica nanocomposites are characterized as a function of conversion degree and normalized particle size, reflecting the degradation of the interphase effect with the parameters considered in this study. The fitted properties of nanocomposites are compared with the MD simulation results and the Mori-Tanaka solutions in **Fig. 10**. The present model accurately describes the thermomechanical properties of epoxy/silica nanocomposites of those obtained from MD simulations with ξ and r_p^* , as given in **Fig. 10**.

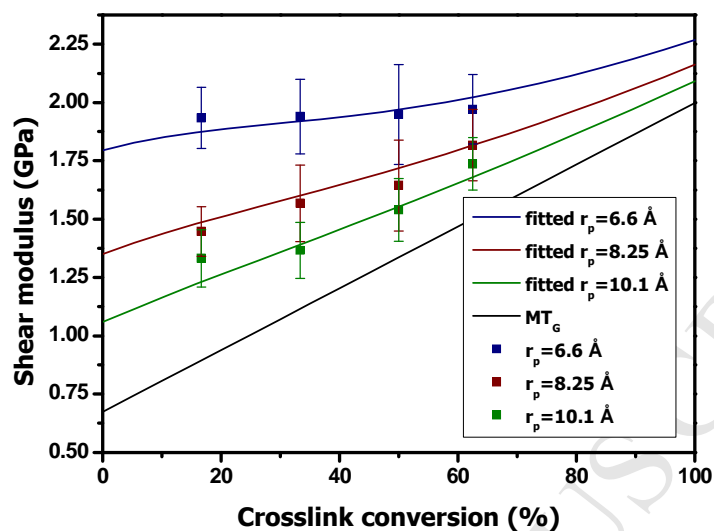
The thermomechanical properties of epoxy nanocomposites are extrapolated to various ranges of crosslink conversions and particle radii under the constant filler volume fraction from the present model as illustrated in **Fig. 11**. The contours for elastic modulus and CTE manifest the nature of the reinforcing effect due to the interphase region in the epoxy/silica nanocomposites. In **Figs. 11(a)** and **11(b)**, as the crosslink conversion increases, the degree of enhancement in elastic moduli decreases, being prominent with increasing particle radius.

Similarly, as can be seen in **Fig. 11(c)**, the reinforcing effect on CTE is notably depressed in highly crosslinked epoxy systems. It is generally agreed that smaller filler inclusions with the same volume fraction of particles having a larger surface area demonstrate higher reinforcing effect on the matrix polymer, especially at the nanoscale, which is termed the ‘particle size effect’. The contours clearly indicate that the particle size effect on the thermomechanical properties due to the presence of the interphase region is disturbed by crosslinking. In other words, the reinforcing effect attributed to the interphase characteristics is hindered by the formation of more crosslinks in the epoxy matrix. To acquire a quantitative understanding of the interphase region, the effective interphase concept is implemented by adopting a 3-phase multi-inclusion model based on the micromechanics regime. The procedures and results are detailed in the following section.

(a)



(b)



(c)

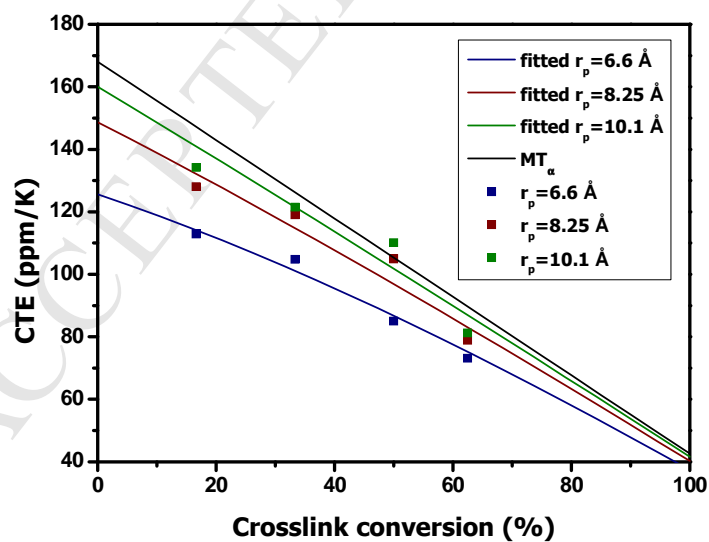
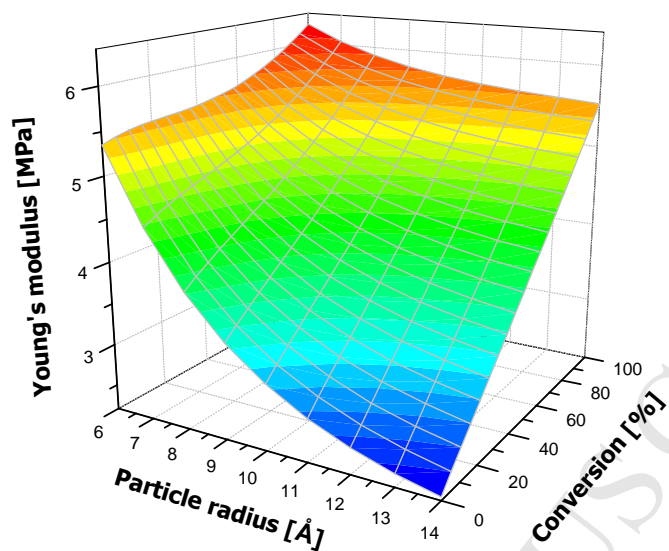
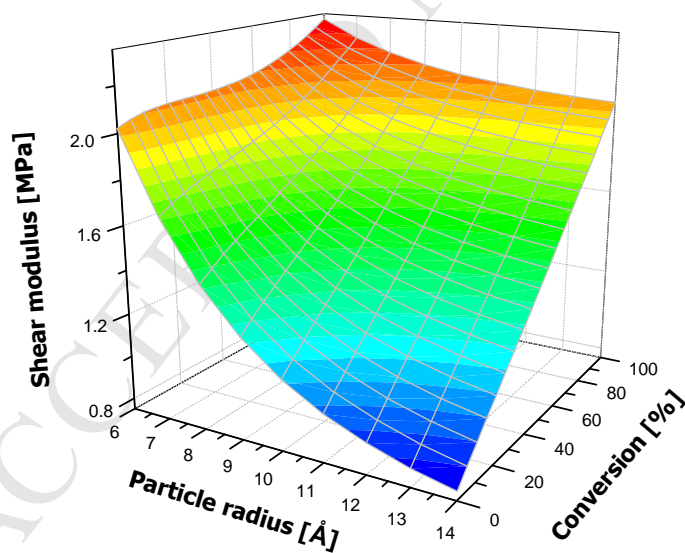


Figure 10. Characterization of thermomechanical properties with crosslink conversion and filler size; (a) Young's modulus, (b) shear modulus, (c) CTE.

(a)



(b)



(c)

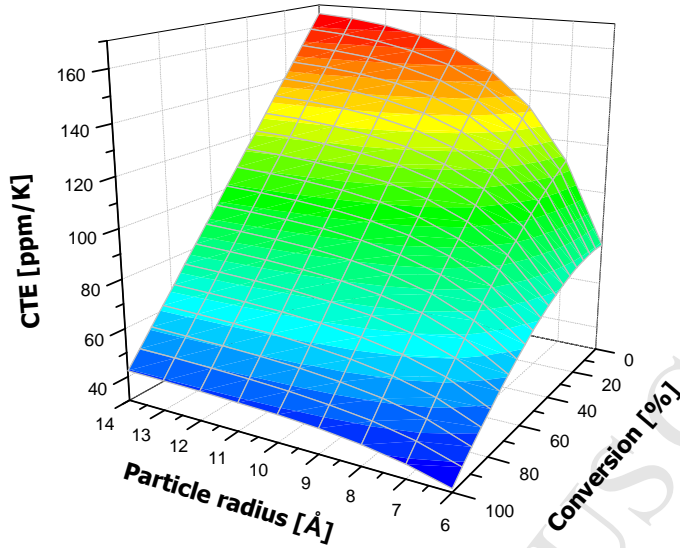


Figure 11. Overall contour of thermomechanical properties with various crosslinking conversions and filler sizes extrapolated from the present analytical model; (a) Young's modulus, (b) shear modulus, (c) CTE.

3.3 Effective interphase concept with the micromechanics-based multi-inclusion model

In order to characterize the interphase behavior, the multi-inclusion model consisting of three-homogeneous and isotropic coaxial phases is implemented. Each phase is embedded into an infinite medium and perfectly bonded to other phases.

The closed form solution of the effective stiffness tensor of the present three-phased model \mathbf{C} is defined as,

$$\mathbf{C} = \mathbf{C}_\infty \left[\mathbf{I} + (\mathbf{S} - \mathbf{I}) (f_p \boldsymbol{\Phi}_p + f_i \boldsymbol{\Phi}_i + f_m \boldsymbol{\Phi}_m) \right] \left[\mathbf{I} + \mathbf{S} (f_p \boldsymbol{\Phi}_p + f_i \boldsymbol{\Phi}_i + f_m \boldsymbol{\Phi}_m) \right]^{-1} \quad (7)$$

where f is the volume fraction of each phase, and the terms in bold typeface refer to the tensor quantities; \mathbf{C}_∞ is the stiffness of the infinite domain, \mathbf{S} and \mathbf{I} are the Eshelby tensor [58] for the spherical inclusion and identity tensor, respectively, and $\boldsymbol{\Phi}$ is the fourth-order eigenstrain concentration tensor of each phase. The subscripts p , i , and m denote

the nanoparticle, interphase, and matrix, respectively. The eigenstrain concentration tensor Φ for the (\bullet) phase is given by,

$$\Phi_{(\bullet)} = \left[\left(\mathbf{C}_\infty - \mathbf{C}_{(\bullet)} \right)^{-1} \mathbf{C}_\infty - \mathbf{S} \right]^{-1}. \quad (8)$$

The overall CTE of the three-phased composites in the multi inclusion model is given as,

$$\alpha = \mathbf{C}^{-1} \mathbf{C}_\infty [\mathbf{I} + \Phi \mathbf{S}]^{-1} \left[f_p (\Phi_p (\mathbf{S} - \mathbf{I}) + \mathbf{I}) : \alpha_p + f_i (\Phi_i (\mathbf{S} - \mathbf{I}) + \mathbf{I}) : \alpha_i + f_m (\Phi_m (\mathbf{S} - \mathbf{I}) + \mathbf{I}) : \alpha_m \right] \quad (9)$$

where $\Phi = \sum_i f_i \Phi_i$.

The volume fraction of the interphase for each nanocomposite was obtained based on the constant thickness of 6.9 Å for simplicity. The stiffness tensor of the infinite medium was defined as $\mathbf{C}_\infty = \mathbf{C}_m$ considering the moderate concentration effect of nanofillers. The stiffness and CTE of the matrix phase are assumed to be the same as those of pure epoxy systems, corresponding to a specific crosslink conversion. The elastic and thermal properties of the interphase can then be calculated using the inverse form of **Eqs. (7)-(9)**. The obtained properties of the interphase will be discussed in detail in a subsequent section. As observed in the previous MD and MM results illustrated in **Figs. 2 and 3**, the interfacial adhesion is likely to be varied with crosslinking degree and particle size. By replacing the filler-matrix interfacial compatibility with a perfect bonding condition between each phase, the interphase properties obtained from the micromechanics model used herein is interpreted as the effective interphase properties [25] which inherently include the variations of both structural characteristics and interfacial compliance with crosslinking and filler size.

Prior to describing the detailed characterization procedure for the interphase properties using the present model, the present model is compared with the simple model, the modified

Halpin-Tsai model [43]. The Halpin-Tsai model [59] is one of the relevant conventional composites models which is based on the self-consistent micromechanics scheme. The modified Halpin-Tsai model was developed by Zare [43] to describe the interphase effect on the elastic property of nanocomposites containing spherical particles (interested reader may refer to the literature for detailed description). Herein, Young's moduli of the interphase were obtained using the modified Halpin-Tsai model, and the values are compared with the present model in **Table. 5**. As can be seen in **Table. 5**, it is obvious that, for the crosslink conversion range considered in this work, the elastic properties of the interphase from the present model and the simple model show significantly reinforced interphase region as compared to the neat epoxy. Moreover, considering the overall trend in the interphase properties with increasing crosslink conversion, the simple model provides a similar trend as observed in the present model; decreasing interphase properties with crosslinking. While both models provide similar interphase properties, the present model leads to slightly higher elastic moduli of the interphase compared to the modified Halpin-Tsai model. This occurrence may be attributed to the semi-empirical assumption on the geometry reinforcement parameter for the spherical inclusion in the Halpin-Tsai model.

Table 5

Comparison of interphase property with the present multi-inclusion model and the modified Halpin-Tsai model [40].

Radius of particle [Å]	Crosslink conversion [%]	Young's modulus of interphase [GPa]	
		Present model	Modified Halpin-Tsai model [40]
6.60	16.66	15.13	11.43
	33.33	10.89	9.17
	50.00	7.78	7.07
	62.50	6.54	6.06
8.25	16.66	12.04	8.85
	33.33	9.54	7.84
	50.00	6.65	5.86
	62.50	6.40	5.74
10.10	16.66	16.98	10.18
	33.33	8.91	6.79
	50.00	6.53	5.50
	62.50	6.91	5.82

3.4 Characterization of interphase property with multiscale modeling

Before describing the detailed process of multiscale modeling of the interphase properties, the overall modeling strategy is illustrated in **Fig. 12**. Based on the result of MD (Composites and neat epoxy systems), the present multi-inclusion model can take into account the thermomechanical properties of the interphase on the basis of the effective interphase concept. To reflect the interphase behavior observed in the atomistic scale, the obtained properties of the interphase zone are functionalized in terms of crosslink conversion and filler size in a similar manner as that applied for the characterization of nanocomposites. The degradation factor for interphase D^i is introduced to represent the variation of the interphase properties $y|_{inter}$ compared to the bulk epoxy region, defined as $D^i = y|_{inter} / y|_{pure}$, based on the

assumption that the interphase properties converge to the bulk epoxy when the interfacial effects vanished. Parameter D' is characterized by two dimensionless variables (ξ and r_p^*) using the same exponential function; the interphase properties can then be expressed as follows.

$$D' = D'(\xi, r_p^*) = 1 + A' \exp[-\alpha' \xi - \beta' r_p^*] \quad (10)$$

$$y|_{inter} = D'(\xi, r_p^*) y|_{pure} = D'(\xi, r_p^*) f(\xi) \quad (11)$$

In a qualitative perspective, D' represents the degree of reinforcing effect on the interphase region compared to the bulk epoxy, showing a proportional relation in the elastic modulus while inversely proportional in CTE. As can be seen in **Fig. 13**, in a lower conversion degree of matrix, the enhancement effect on the stiffness and thermal stability of the interphase zone (increase in elastic modulus and decrease in CTE) is relatively more significant than that in a highly crosslinked matrix. In **Fig. 14**, the elastic modulus and CTE of the interphase region are modeled using **Eqs. (10)** and **(11)**, and are compared with the crosslinked bulk epoxy matrix. For a fixed crosslink conversion, the smaller filler inclusions induce higher interphase properties in terms of stiffness and thermal stability. Moreover, as the crosslinking in epoxy proceeds further, the interphase properties tend to decrease.

Although the effective interphase concept does not specifically distinguish between the interphase property and the interfacial compliance, it can be implemented in a continuum model to reflect the degradation of the interphase effect with increasing crosslinking as well as embedded particle size. According to the present multi-inclusion model, the elastic modulus and CTE of composites as given in **Eqs. (7)-(9)** can be defined as the following,

$$\begin{aligned} \mathbf{C} &= \mathbf{C}(\mathbf{C}_p, \mathbf{C}_m, \mathbf{C}_i, f_p, f_m, f_i) \\ \alpha &= \alpha(\mathbf{C}_p, \mathbf{C}_m, \mathbf{C}_i, \alpha_p, \alpha_m, \alpha_i, f_p, f_m, f_i) \end{aligned} \quad (12)$$

Herein, the effective interphase has been characterized as $\mathbf{C}_i = \mathbf{C}(\xi, r_p^*)$ and $\alpha_i = \alpha(\xi, r_p^*)$, which represent the variation of elastic modulus and CTE of the interphase region and the interfacial compliance, respectively. Together with the assumption that the property of the epoxy matrix is the same as that of neat epoxy, $\mathbf{C}_m = \mathbf{C}(\xi)$ and $\alpha_m = \alpha(\xi)$, the thermomechanical properties can be predicted from the micromechanics-based multi-inclusion model using **Eqs. (7)-(9)** with the incorporation of the effective interphase. **Fig. 15** shows a comparison of the micromechanics prediction with the results from MD simulations and the curve fit of the present model. As can be seen in **Fig. 15**, the micromechanics predictions from the effective interphase and the modeled matrix property show a reasonable agreement with the present model.

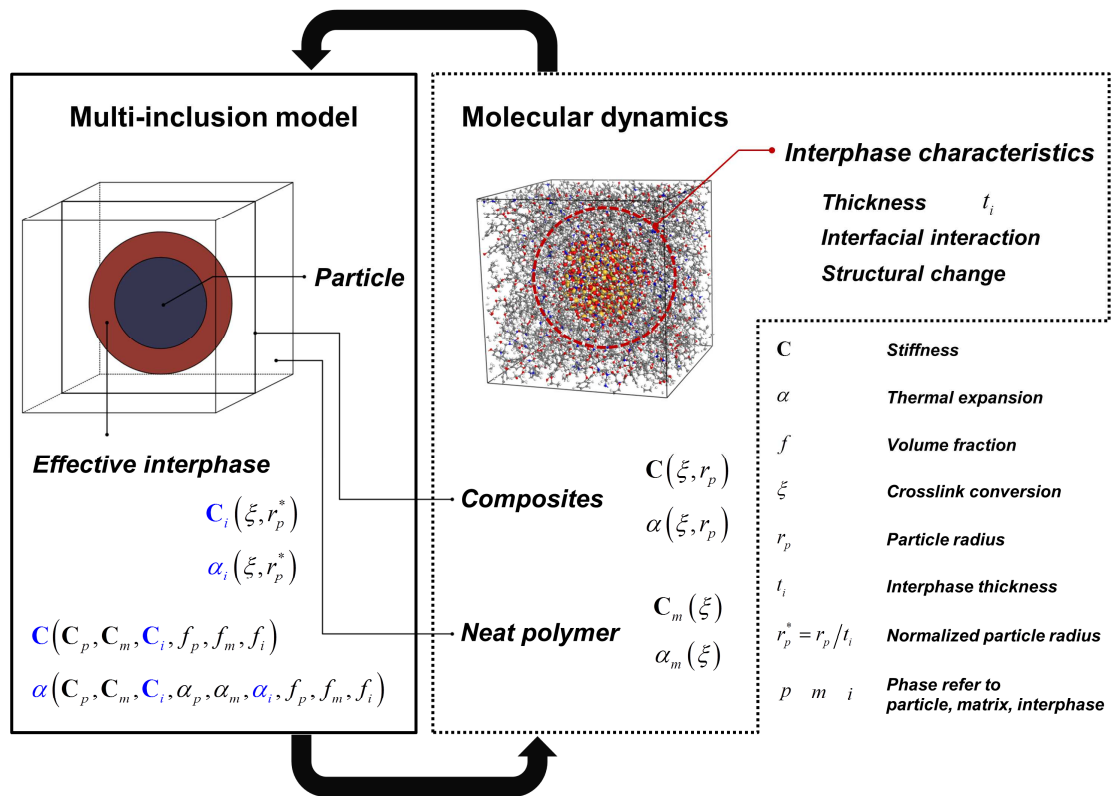
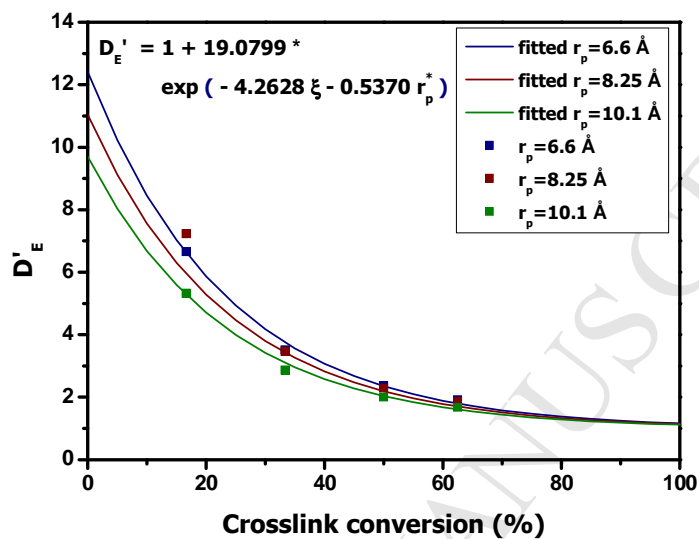
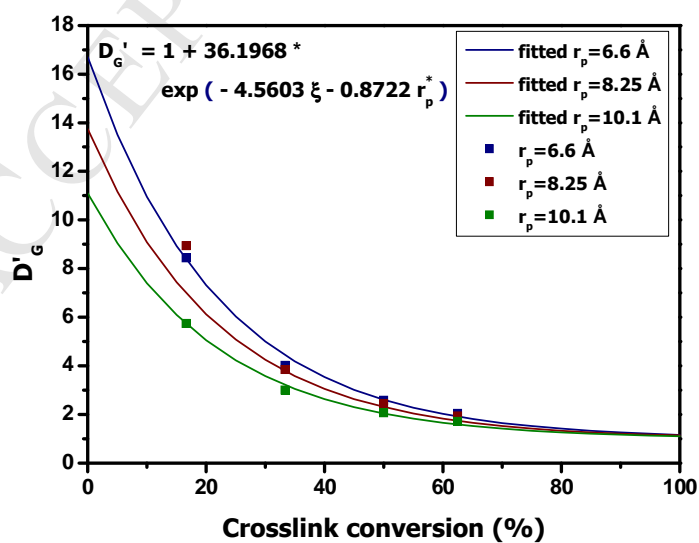


Figure 12. Overall schematic of the multiscale modeling of the interphase property; blue-colored terms (For interpretation of the references to color in this figure legend, the reader is referred to the web version of the article.) indicate the values predicted from the multi-inclusion model.

(a)



(b)



(c)

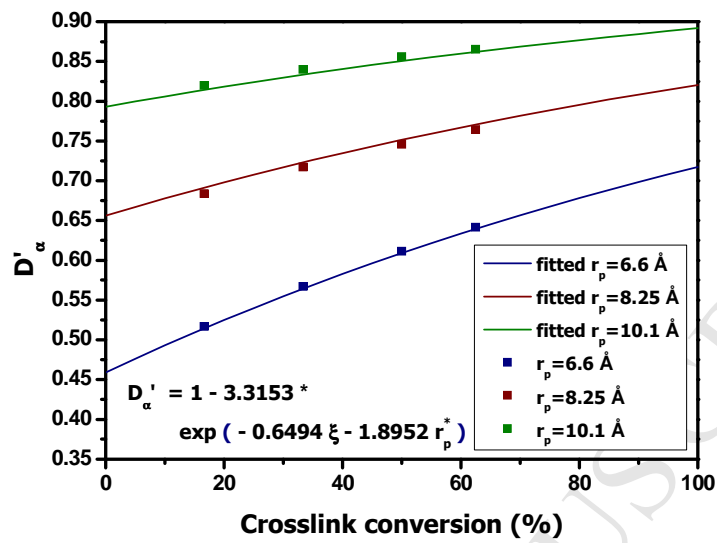
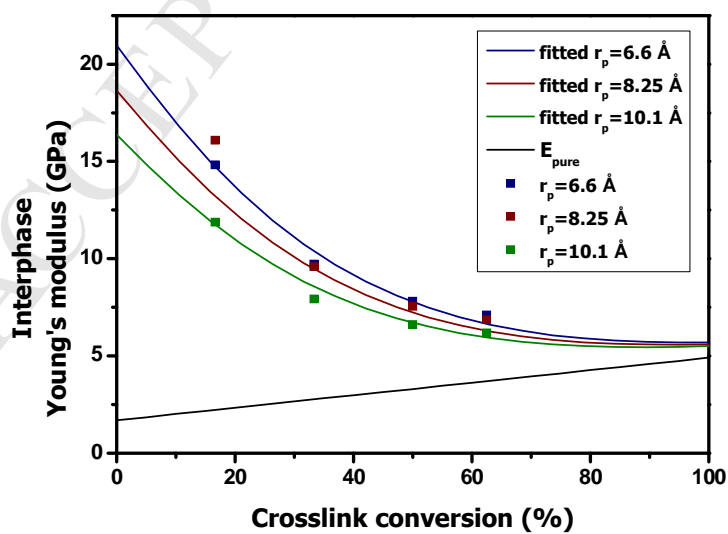
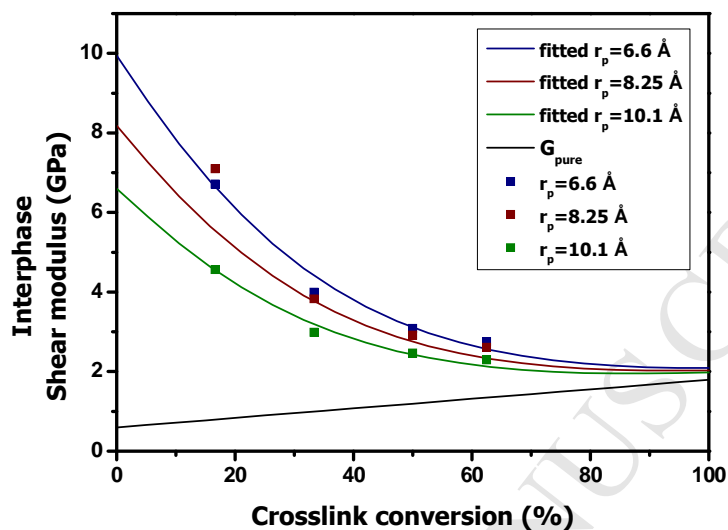


Figure 13. Characterization of degradation factor of interphase D' for (a) Young's modulus D'_E , (b) shear modulus D'_G , and (c) CTE D'_α with a curve fit by the equation $D'(\xi, r_p^*) = 1 + A' \exp[-\alpha' \xi - \beta' r_p^*]$.

(a)



(b)



(c)

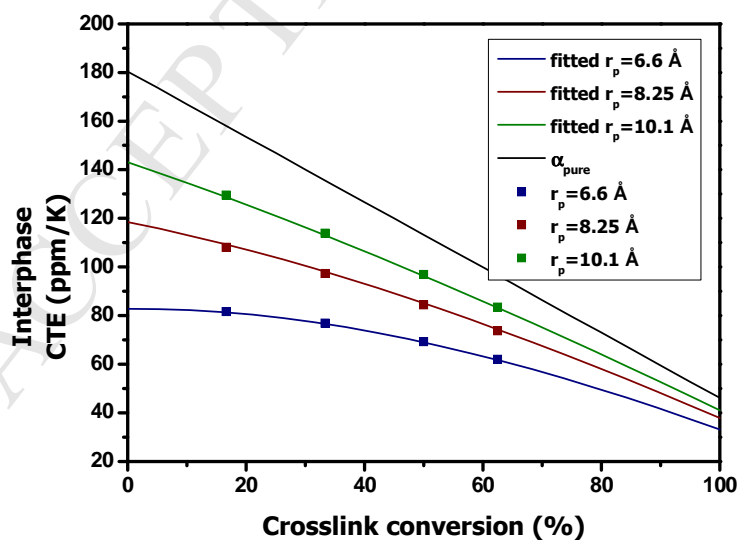
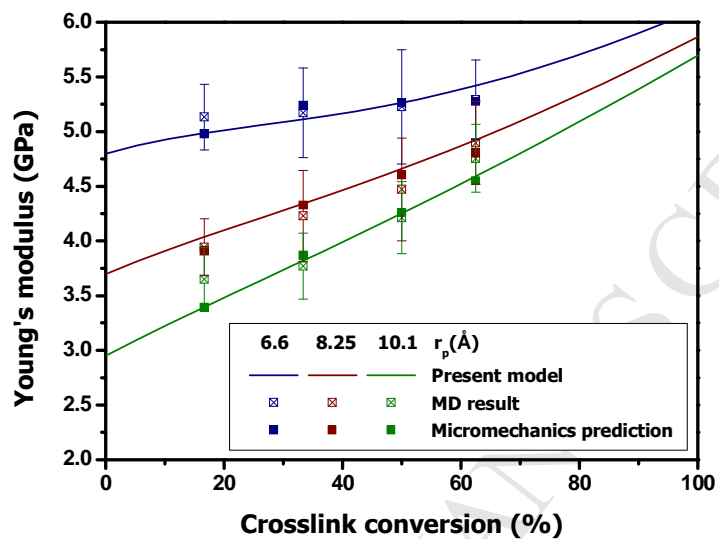
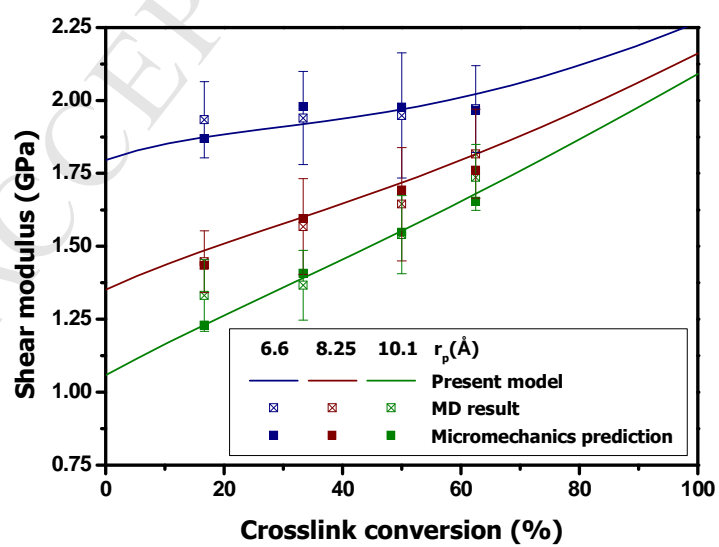


Figure 14. Characterization of interphase properties with crosslink conversion and filler size: (a) Young's modulus, (b) shear modulus, (c) CTE.

(a)



(b)



(c)

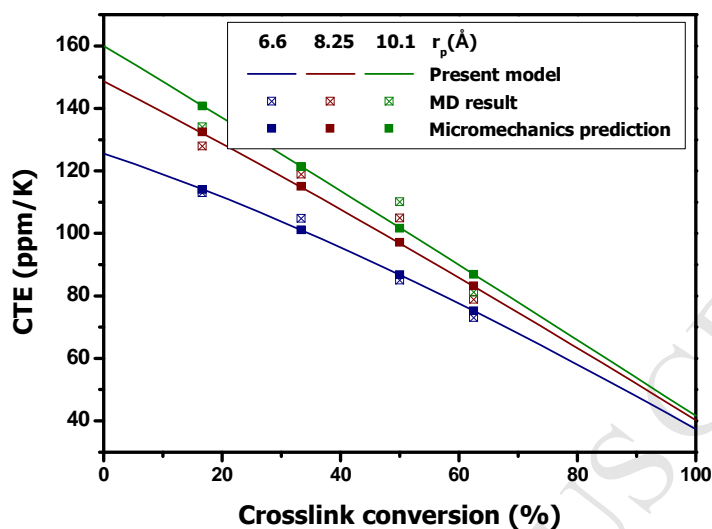


Figure 15. Micromechanics prediction of elastic modulus and CTE compared to MD result and present model.

4. Conclusion

Atomic simulations were performed to investigate the interfacial characteristics of epoxy/silica nanocomposites with the crosslinking conversions of epoxy matrix. The results of MD and MM simulations demonstrate that the nature of the interfacial interactions between the silica and epoxy matrix show a clear dependency with the degree of crosslinking; the interfacial adhesions are substantially disturbed with the formation of further crosslinks in the epoxy, resulting in disturbed enhancing effects on stiffness and thermal stability with crosslinking. As far as the structural conformation change of the interphase with the conversion degree is concerned, important features were observed supporting the reduction of interfacial characteristics. The results of the radial mass density profiles, the local crosslinks distributions, and the free volumes at the filler surface consistently demonstrate that the structural characteristics are substantially influenced by the nature of interfacial communication with the crosslink conversion. Since the behavior of the interphase zone is

strongly governed by the interfacial communication at the filler surface, the variations of interfacial characteristics with crosslinking need to be taken into account to understand the interphase of epoxy nanocomposite systems as well as their reinforcing mechanism. In this work, together with profound considerations of varying crosslink conversion and filler size in epoxy nanocomposites, a multiscale scheme to characterize the interphase region is proposed with the incorporation of molecular simulations and a micromechanics-based continuum model. Based on the findings of the atomistic simulations, the elastic modulus and CTE of nanocomposites are characterized in terms of crosslink conversion and normalized filler size. From the modeled thermomechanical properties of epoxy/silica nanocomposites, the interphase zone is further characterized with the aid of the multi-inclusion continuum model. The effective interphase zone is addressed to reflect the variations of interfacial adhesion and the interphase property. The degradation of the effective interphase zone is modeled with crosslink conversion and filler size. The micromechanics predictions from the effective interphase for the thermomechanical properties of nanocomposites are confirmed and compared to the MD results and the present model for composites.

From the multiscale framework presented herein, the information at the molecular level regarding the interphase region of epoxy nanocomposites is transferred to the equivalent continuum model. Addressing the effective interphase concept, the interphase properties obtained from the present multi-inclusion model are termed as an effective interphase property. Since a perfect interfacial bonding condition is applied in the continuum model, the effective interphase property is not an independent property of the interphase but an effective property which reflects the variations of both structural and interfacial characteristics with the crosslink conversion and particle size. However, the present multiscale modeling using the effective interphase concept will serve as an efficient bridging scheme to understand the

complex interfacial nature of crosslinked epoxy composite systems and their structure-property relationship, providing a design guideline for epoxy nanocomposites in their static property (elastic modulus and CTE) on the basis of the detailed interphase characteristics with varying crosslink conversions and particle sizes. The multiscale modeling scheme proposed herein can be further extended to the various multifunctional characteristics and the dynamic behavior with a profound consideration of the interfacial region in the nanocomposites system.

Acknowledgments

This work was supported by the National Research Foundation of Korea(NRF) grant funded by the Korea government(MSIP) (No. 2012R1A3A2048841).

References

- [1] Li C, Strachan A. Molecular scale simulations on thermoset polymers: A review. *Journal of Polymer Science Part B: Polymer Physics*. 2015;53(2):103-22.
- [2] Zeng QH, Yu AB, Lu GQ. Multiscale modeling and simulation of polymer nanocomposites. *Progress in Polymer Science*. 2008;33(2):191-269.
- [3] Jancar J, Douglas JF, Starr FW, Kumar SK, Cassagnau P, Lesser AJ, et al. Current issues in research on structure-property relationships in polymer nanocomposites. *Polymer*. 2010;51(15):3321-43.
- [4] Chan M-l, Lau K-t, Wong T-t, Ho M-p, Hui D. Mechanism of reinforcement in a nanoclay/polymer composite. *Composites Part B: Engineering*. 2011;42(6):1708-12.
- [5] Rahul R, Kitey R. Effect of cross-linking on dynamic mechanical and fracture behavior of epoxy variants. *Composites Part B: Engineering*. 2016;85:336-42.

- [6] Putz KW, Palmeri MJ, Cohn RB, Andrews R, Brinson LC. Effect of Cross-Link Density on Interphase Creation in Polymer Nanocomposites. *Macromolecules*. 2008;41(18):6752-6.
- [7] Hadden CM, Jensen BD, Bandyopadhyay A, Odegard GM, Koo A, Liang R. Molecular modeling of EPON-862/graphite composites: Interfacial characteristics for multiple crosslink densities. *Composites Science and Technology*. 2013;76(0):92-9.
- [8] Li M, Gu Y-Z, Liu H, Li Y-X, Wang S-K, Wu Q, et al. Investigation the interphase formation process of carbon fiber/epoxy composites using a multiscale simulation method. *Composites Science and Technology*. 2013;86(0):117-21.
- [9] Ghanbari A, Rahimi M, Dehghany J. Influence of Surface Grafted Polymers on the Polymer Dynamics in a Silica–Polystyrene Nanocomposite: A Coarse-Grained Molecular Dynamics Investigation. *The Journal of Physical Chemistry C*. 2013;117(47):25069-76.
- [10] Ramanathan T, Liu H, Brinson LC. Functionalized SWNT/polymer nanocomposites for dramatic property improvement. *Journal of Polymer Science Part B: Polymer Physics*. 2005;43(17):2269-79.
- [11] Ahmadi M, Masoomi M, Safi S. Mechanical property characterization of carbon nanofiber/epoxy nanocomposites reinforced by GMA-grafted UHMWPE fibers. *Composites Part B: Engineering*. 2015;83:43-9.
- [12] Gojny FH, Schulte K. Functionalisation effect on the thermo-mechanical behaviour of multi-wall carbon nanotube/epoxy-composites. *Composites Science and Technology*. 2004;64(15):2303-8.
- [13] Zhamu A, Hou Y, Zhong W-H, Stone JJ, Li J, Lukehart CM. Properties of a reactive-graphitic-carbon-nanofibers-reinforced epoxy. *Polymer Composites*. 2007;28(5):605-11.
- [14] Fidelus JD, Wiesel E, Gojny FH, Schulte K, Wagner HD. Thermo-mechanical properties of randomly oriented carbon/epoxy nanocomposites. *Composites Part A: Applied Science and*

Manufacturing. 2005;36(11):1555-61.

[15] Liu G, Zhang H, Zhang D-j, Zhang H, Zhang Z, An X-f, et al. On depression of glass transition temperature of epoxy nanocomposites. *JOURNAL OF MATERIALS SCIENCE*. 2012;47(19):6891-5.

[16] Sun Y, Zhang Z, Moon K-S, Wong CP. Glass transition and relaxation behavior of epoxy nanocomposites. *Journal of Polymer Science Part B: Polymer Physics*. 2004;42(21):3849-58.

[17] Harton SE, Kumar SK, Yang H, Koga T, Hicks K, Lee H, et al. Immobilized Polymer Layers on Spherical Nanoparticles. *Macromolecules*. 2010;43(7):3415-21.

[18] Tsai J-L, Tzeng S-H, Chiu Y-T. Characterizing elastic properties of carbon nanotubes/polyimide nanocomposites using multi-scale simulation. *Composites Part B: Engineering*. 2010;41(1):106-15.

[19] Olmos D, Prolongo SG, González-Benito J. Thermo-mechanical properties of polysulfone based nanocomposites with well dispersed silica nanoparticles. *Composites Part B: Engineering*. 2014;61:307-14.

[20] Ionita M. Multiscale molecular modeling of SWCNTs/epoxy resin composites mechanical behaviour. *Composites Part B: Engineering*. 2012;43(8):3491-6.

[21] Maleki Moghadam R, Saber-Samandari S, Hosseini SA. On the tensile behavior of clay–epoxy nanocomposite considering interphase debonding damage via mixed-mode cohesive zone material. *Composites Part B: Engineering*. 2016;89:303-15.

[22] Rahman R, Haque A. Molecular modeling of crosslinked graphene–epoxy nanocomposites for characterization of elastic constants and interfacial properties. *Composites Part B: Engineering*. 2013;54:353-64.

[23] Zhang Y, Zhuang X, Muthu J, Mabrouki T, Fontaine M, Gong Y, et al. Load transfer of graphene/carbon nanotube/polyethylene hybrid nanocomposite by molecular dynamics

simulation. *Composites Part B: Engineering*. 2014;63:27-33.

[24] Li C, Browning AR, Christensen S, Strachan A. Atomistic simulations on multilayer graphene reinforced epoxy composites. *Composites Part A: Applied Science and Manufacturing*. 2012;43(8):1293-300.

[25] Kim B, Choi J, Yang S, Yu S, Cho M. Influence of crosslink density on the interfacial characteristics of epoxy nanocomposites. *Polymer*. 2015;60:186-97.

[26] Langeloth M, Sugii T, Böhm MC, Müller-Plathe F. Formation of the Interphase of a Cured Epoxy Resin Near a Metal Surface: Reactive Coarse-Grained Molecular Dynamics Simulations. *Soft Materials*. 2014;12(sup1):S71-S9.

[27] Odegard GM, Clancy TC, Gates TS. Modeling of the mechanical properties of nanoparticle/polymer composites. *Polymer*. 2005;46(2):553-62.

[28] Yang S, Cho M. Scale bridging method to characterize mechanical properties of nanoparticle/polymer nanocomposites. *Applied Physics Letters*. 2008;93(4):-.

[29] Yu S, Yang S, Cho M. Multi-scale modeling of cross-linked epoxy nanocomposites. *Polymer*. 2009;50(3):945-52.

[30] Yang S, Cho M. A scale-bridging method for nanoparticulate polymer nanocomposites and their nondilute concentration effect. *Applied Physics Letters*. 2009;94(22):223104.

[31] Safaei M, Sheidaei A, Baniassadi M, Ahzi S, Mosavi Mashhadi M, Pourboghrat F. An interfacial debonding-induced damage model for graphite nanoplatelet polymer composites. *Computational Materials Science*. 2015;96, Part A:191-9.

[32] Amnaya PA, Dimitris CL, Daniel CH. Modeling of graphene–polymer interfacial mechanical behavior using molecular dynamics. *Modelling and Simulation in Materials Science and Engineering*. 2009;17(1):015002.

[33] Zappalorto M, Salviato M, Quaresimin M. Influence of the interphase zone on the

nanoparticle debonding stress. *Composites Science and Technology*. 2011;72(1):49-55.

[34] Accelrys Inc., San Diego, www.Accelrys.com

[35] Sun H. COMPASS: An ab Initio Force-Field Optimized for Condensed-Phase Applications Overview with Details on Alkane and Benzene Compounds. *The Journal of Physical Chemistry B*. 1998;102(38):7338-64.

[36] Parrinello M, Rahman A. Crystal structure and pair potentials: A molecular-dynamics study. *Physical Review Letters*. 1980;45:1196-9.

[37] Parrinello M, Rahman A. Strain fluctuations and elastic constants. *The Journal of chemical physics*. 1982;76(5):2662-6.

[38] Yang S, Yu S, Cho M. Sequential thermoelastic multiscale analysis of nanoparticulate composites. *Journal of Applied Physics*. 2010;108(5):056102.

[39] Shin H, Chang S, Yang S, Youn BD, Cho M. Statistical multiscale homogenization approach for analyzing polymer nanocomposites that include model inherent uncertainties of molecular dynamics simulations. *Composites Part B: Engineering*. 2016;87:120-31.

[40] Connolly M. Solvent-accessible surfaces of proteins and nucleic acids. *Science*. 1983;221(4612):709-13.

[41] Connolly M. Analytical molecular surface calculation. *Journal of Applied Crystallography*. 1983;16(5):548-58.

[42] Li C, Strachan A. Free volume evolution in the process of epoxy curing and its effect on mechanical properties. *Polymer*. 2016;97:456-64.

[43] Zare Y. Development of Halpin-Tsai model for polymer nanocomposites assuming interphase properties and nanofiller size. *Polymer Testing*. 2016;51:69-73.

[44] Zare Y. Assumption of interphase properties in classical Christensen-Lo model for Young's modulus of polymer nanocomposites reinforced with spherical nanoparticles. *RSC*

Advances. 2015;5(116):95532-8.

[45] Ji XL, Jing JK, Jiang W, Jiang BZ. Tensile modulus of polymer nanocomposites. *Polymer Engineering & Science*. 2002;42(5):983-93.

[46] Quaresimin M, Salviato M, Zappalorto M. A multi-scale and multi-mechanism approach for the fracture toughness assessment of polymer nanocomposites. *Composites Science and Technology*. 2014;91(0):16-21.

[47] Zappalorto M, Salviato M, Quaresimin M. A multiscale model to describe nanocomposite fracture toughness enhancement by the plastic yielding of nanovoids. *Composites Science and Technology*. 2012;72(14):1683-91.

[48] Salviato M, Zappalorto M, Quaresimin M. Plastic shear bands and fracture toughness improvements of nanoparticle filled polymers: A multiscale analytical model. *Composites Part A: Applied Science and Manufacturing*. 2013;48:144-52.

[49] Upadhyaya P, Kumar S. Micromechanics of stress transfer through the interphase in fiber-reinforced composites. *Mechanics of Materials*. 2015;89:190-201.

[50] Jia Z, Ma H-l, Cheng L-K, Lau K-t, Hui D, Yuan G. Stress transfer properties of carbon nanotube reinforced polymer composites at low temperature environments. *Composites Part B: Engineering*. 2016;106:356-65.

[51] Spanos KN, Georgantzinou SK, Anifantis NK. Investigation of stress transfer in carbon nanotube reinforced composites using a multi-scale finite element approach. *Composites Part B: Engineering*. 2014;63:85-93.

[52] Rao Y-N, Dai H-L. Micromechanics-based thermo-viscoelastic properties prediction of fiber reinforced polymers with graded interphases and slightly weakened interfaces. *Composite Structures*. 2017;168:440-55.

[53] Gupta VB, Drzal LT, Lee CYC, Rich MJ. The temperature-dependence of some

mechanical properties of a cured epoxy resin system. *Polymer Engineering & Science*. 1985;25(13):812-23.

[54] Bandyopadhyay A, Valavala PK, Clancy TC, Wise KE, Odegard GM. Molecular modeling of crosslinked epoxy polymers: The effect of crosslink density on thermomechanical properties. *Polymer*. 2011;52(11):2445-52.

[55] Subramanian N, Rai A, Chattopadhyay A. Atomistically informed stochastic multiscale model to predict the behavior of carbon nanotube-enhanced nanocomposites. *Carbon*. 2015;94:661-72.

[56] Li C, Strachan A. Evolution of network topology of bifunctional epoxy thermosets during cure and its relationship to thermo-mechanical properties: A molecular dynamics study. *Polymer*. 2015;75:151-60.

[57] Shenogina NB, Tsige M, Patnaik SS, Mukhopadhyay SM. Molecular Modeling Approach to Prediction of Thermo-Mechanical Behavior of Thermoset Polymer Networks. *Macromolecules*. 2012;45(12):5307-15.

[58] Eshelby JD. The determination of the elastic field of an ellipsoidal inclusion, and related problems. *Proceedings of the Royal Society of London Series A Mathematical and Physical Sciences*. 1957;241(1226):376-96.

[59] Affdl JCH, Kardos JL. The Halpin-Tsai equations: A review. *Polymer Engineering & Science*. 1976;16(5):344-52.